IEEE Photonics Journal
An IEEE Photonics Society Publication

Open Access

In Situ Calibration of Magnetic Coil System Using Ellipticity-Induced Bell-Bloom Magnetometer

Volume 11, Number 1, February 2019

Guiying Zhang
Shengjie Huang
Qiang Lin

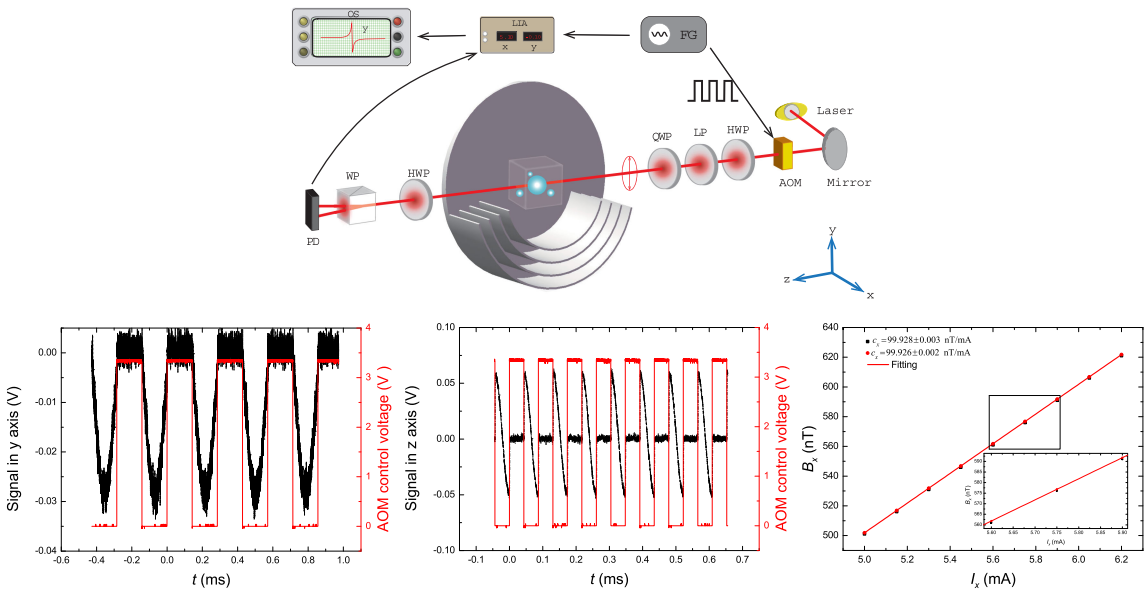

DOI: 10.1109/JPHOT.2018.2889578
1943-0655

In Situ Calibration of Magnetic Coil System Using Ellipticity-Induced Bell-Bloom Magnetometer

Guiying Zhang, Shengjie Huang, and Qiang Lin

Collaborative Innovation Center for Bio-Med Physics Information Technology, College of Science, Zhejiang University of Technology, Hangzhou 310023, China

DOI:10.1109/JPHOT.2018.2889578

Manuscript received November 1, 2018; accepted December 19, 2018. Date of publication December 24, 2018; date of current version January 9, 2019. This work was supported in part by the National Key Research and Development Program of China under Grant 2017YFC0601602 and in part by the National Natural Science Foundation of China under Grant 11704335, Grant 61727821, and Grant 61475139. Corresponding author: Qiang Lin (e-mail: qlin@zjut.edu.cn).

Abstract: The three-axis coil system is most commonly used in magnetic field measurement. The coil constant is an important parameter. We demonstrate a method to measure the coil constant based on the Larmor frequency. An elliptically polarized light is used to simultaneously excite the spin orientation and spin alignment via synchronous optical pumping. And then the coil system can be calibrated by measuring the magnetic resonance frequency of Bell-Bloom magnetometer. The advantage of this method is that the coil constants of all three directions can be obtained without any active adjustments. It is important for some applications, such as measuring the biological magnetic field with the integrated magnetometer. The method for calibration of a three-axis coil system is experimentally exploited. The experimental results show that the calibration accuracy of pT level can be achieved.

Index Terms: Bell-Bloom magnetometer, elliptically polarized light, coil calibration.

1. Introduction

Optically pumped atomic magnetometer has been actively developed in recent years [1]–[4], which is widely used in many applications, such as biomagnetism [5], [6], low-field magnetic resonance [7], [8], searching for dark matter [9] and probing fundamental symmetries [10]. All these applications usually need to be operated under the clean magnetic environment, which can be achieved by a multilayer magnetic shield and a triaxial magnetic coil. The multilayer magnetic shield is used to reduce the earth field from 30000 nT to only several nT [11]. And the triaxial magnetic coil is used to generate the necessary homogeneous magnetic field in the center along the x, y or z direction, such as magnetocardiography measurement using Mx magnetometer [12]. In principle, magnetic field strength and distribution can be calculated from the known coil geometry using some magnetic simulation software. However, the presence of the high permeability shielding materials can distort the magnetic field generated by the coils. This effect makes it difficult to obtain information about magnetic field by quantitative simulation. Therefore, it is important to find a method to calibrate the coils in situ precisely.

Traditionally, a fluxgate magnetometer is used to calibrate the magnetic field coils, but subject to the precision limit, the calibration accuracy of the method is unsatisfactory. In addition, there is another problem of position error, because the fluxgate magnetometer may not be put in the

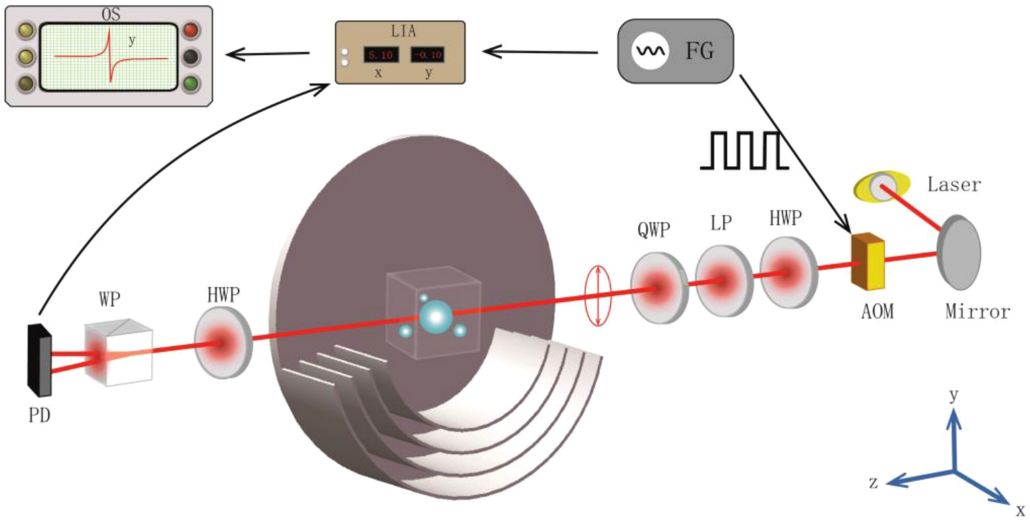

Fig. 1. Schematic diagram of the experimental setup. AOM, acoustic optical modulator; HWP, half-wave plate; LP, linear polarizer; QWP, quarter-wave plate; WP, Wollaston prim; PD, balanced photodetector; FG, function generator; LIA, lock-in amplifier; OS, oscilloscope.

exact same place as the atomic vapor. Therefore, the best way to measure the coil constants is to use the atomic vapor itself. In recent years, there are already several methods developed. One method exploits the FID signal of alkali atoms or the hyperpolarized noble atoms to derive the Larmor precession frequency, and then measures the coil constants based on the Larmor precession frequency [13], [14]. Another method calibrates the coils by measuring the magnetic resonance frequency of the Cs atoms using Mx magnetometer [15]. All these methods can measure the magnetic field coils accurately. However, they suffer from the same problem, i.e., for a certain direction coil, the coil constant can not be measured directly without active adjustments. But in certain situations, it is impossible to adjust the system elements, especially for the integrated magnetometer systems. For example, a fully integrated magnetometer expected to be applied to magnetoencephalography is demonstrated [16]. An elliptically polarized light has been used as the pump and probe light simultaneously to enhance the amplitude of spin exchange relaxation free magnetometer. In this integrated system, the sensor arrangement can't be changed freely.

In this paper, a new elliptically-induced Bell-Bloom magnetometer is put forward and exploited to calibrate the coils of all three directions without any adjustments. The elliptically polarized light is used to simultaneously excite the spin orientation and spin alignment via synchronous optical pumping. When the magnetic field is along the x or y direction, transverse to the light propagation direction, the spin orientation Bell-Bloom magnetometer works. In contrast, when the magnetic field is parallel to the z axis, the orientation does not process. This is a dead zone for the spin orientation Bell-Bloom magnetometer. However, in this case, the spin alignment processes, which results in the spin alignment Bell-Bloom magnetic resonance. Based on this, the Bell-Bloom magnetometer with amplitude modulated elliptically polarized light also have the potential to measure the magnetic field in all directions. A different modulation method with similar effect has been demonstrated by M.V Romalis *et al.* which uses the polarization modulated light to eliminate the dead zone effect [17].

2. Experimental Setup

The experimental set up is schematically illustrated in Fig. 1. A cubic Pyrex cell (24 mm $\times$ 24 mm $\times$ 24 mm) containing isotopically enriched Rb (99.5% ^{87}Rb) is used in this experiment. The inner surface of the cell was coated with Octadecyltrichlorosilane (OTS), which can reduce the wall

relaxation. The vapor cell also contained 5 torr N_2 quenching gas to increase the optical pumping efficiency by velocity changing collisions. The cell temperature is stabilized at room temperature, corresponding to the Rb density of about 5×10^9 atoms/cm^3. The vapor cell is mounted at the center of the coil system nested within the innermost layer of a five-layer cylindrical μ-metal shield. The coil system can provide a homogeneous magnetic field within the volume of the cell in all three directions. The optical configuration is simple, only one light beam produced by a tunable external-cavity diode laser (Toptica DL Pro) is used. The light beam passes through a half-wave plate, a linear polarizer and a quarter-wave plate, and then enters the vapor cell. The frequency of the light is red detuned by 250 MHz from the $F = 2 \rightarrow F' = 1$ transition. The intensity is square-wave modulated by an acoustic optical modulator (AOM) controlled by a function generator, and the major axis of the polarization ellipse is adjusted to be along the y axis. Prior to entering the vapor cell, the polarization of the light is measured by a SK polarization analyzer, and the polarization analyzer will be removed before the experiment. The light beam is expanded to 10 mm in diameter to eliminate the wall-induced Ramsey effect. The paramagnetic Faraday rotation is measured with polarization homodyning consisting of a Wollaston prism and a balanced photodetector. Subsequently the homodyne output is sent into the input of a Stanford lock-in amplifier referenced to the AOM modulation frequency.

3. Theoretical Model

The basic experimental configuration of the elliptically-induced Bell-Bloom magnetometer has been shown in Fig. 1. The elliptically polarized light propagates along the z axis whose intensity is modulated by a 50% duty cycle square wave with 100% modulation depth. When the magnetic field is along the y direction, the dynamics of the spin orientation polarization is governed by the Bloch equations [18]:

$$\frac{dP_+}{dt} = -iP_+\omega_L - \Gamma P_+ + R(t), \tag{1}$$

where $P_+ = P_z + iP_x$, is the components of the spin orientation polarization P that transverse to the magnetic field. Γ is the total transverse relaxation rate which includes the optical pumping relaxation rate, spin exchange relaxation rate and wall relaxation rate, here Γ can be regarded as time independent due to small pumping rate. We assume the square wave amplitude modulation of the light beam is symmetrical about time zero, so that the Fourier series expansion of the optical pumping rate $R(t)$ is given by

$$R(t) = \frac{R_0}{2} + \sum_{n=1}^{\infty} \frac{2R_0}{n\pi} \sin\left(\frac{n\pi}{2}\right) \cos(n\omega t), \tag{2}$$

where R_0 is the amplitude of the square wave pumping rate, ω is the modulation frequency. Expand $P_+ = \sum_{n=-\infty}^{+\infty} P_+^n \exp(-in\omega t)$, substitute (2) into (1), and solve the equation. Then the steady state solution is obtained,

$$P_+ = \sum_{n=-\infty}^{+\infty} \frac{\mathrm{sinc}(n\pi/2)R_0/2}{i(\omega_L - n\omega) + \Gamma} \exp(-in\omega t). \tag{3}$$

When the modulation frequency matches the Larmor frequency, the amplitude of the 1st harmonic is resonantly enhanced over the other high-order harmonics and is given by $P_+^1 = \nu + i\mu$ with

$$\nu = \frac{\Gamma R_0/\pi}{(\omega_L - \omega)^2 + \Gamma^2}, \mu = -\frac{(\omega_L - \omega)R_0/\pi}{(\omega_L - \omega)^2 + \Gamma^2}. \tag{4}$$

The line shapes of ν and μ are absorptive and dispersive Lorentzian profiles after demodulation, respectively. From (4), one can find that the magnetic resonance appears at $\omega = \omega_L$. And thus the 1st harmonic z component of the polarization is $P_z^1 = \nu\cos(\omega t) + \mu\sin(\omega t)$. Except for the 1st harmonic, the orientation polarization also contains an unmodulated DC Lorentzian (Hanle)

resonance centered at $\omega_L = 0$, that is,

$$P_z^0 = \frac{\Gamma R_0/2}{\omega_L^2 + \Gamma^2}. \tag{5}$$

The precession of the transverse polarization is detected by the paramagnetic Faraday rotation using the same intensity modulated light. Therefore, the polarimeter signal is a convolution of the light intensity modulation and orientation polarization induced optical rotation,

$$S_z(y) = \beta\left[P_z^0 + \nu\cos(\omega t) + \mu\sin(\omega t)\right] I(t), \tag{6}$$

where β is the proportional coefficient, $I(t)$ is the square-wave modulated intensity which has the similar Fourier series expansion with $R(t)$. The same results can be obtained in the x direction.

When the magnetic field is applied along the z direction, spin alignment instead of spin orientation is generated via synchronous optical pumping. According to the similar solving procedure of (1)–(6), the polarimeter signal of the alignment polarization can be obtained as follows:

$$S_z(z) = \beta\left[A_y^0 + \nu\sin(\omega t) + \mu\cos(\omega t)\right] I(t). \tag{7}$$

The solving procedure of (7) is omitted for brevity. Comparing (6) and (7), there is a 90° phase shift between the polarimeter signal of spin alignment and that of spin orientation. The origin of the phase shift can be found in Ref. [19]. The zero-order component of the alignment polarization A_y^0 has the similar formula described as the P_z^0. ν and μ can also be described by equation (4). But in the alignment polarization, the magnetic resonance occurs at $\omega = 2\omega_L$. Therefore, ω_L should be replaced by $2\omega_L$ in these formulas. In addition, equation (7) shows that the DC offset will be mixed into the dispersive signal, causing a base floor.

For a given signal noise δS_z, the resulting sensitivity δB of the magnetometer is [20]

$$\delta B = \frac{\delta S_z}{\gamma k_0}, \tag{8}$$

where γ is the gyromagnetic ratio, $k_0 \propto \partial\mu/\partial\omega(\omega = \omega_L \text{ or } \omega = \omega_{2L})$ is the frequency response at resonance.

4. Experimental Results and Analysis

At first, let us consider the magnetic field along the y direction. The square-wave modulation light gives the time domain signal as shown in Fig. 2(a), where the modulation frequency ω is synchronized with the Larmor frequency ω_L. The experimental signal agrees with the prediction of (6). The signal is demodulated with lock-in amplifier to extract the quadrature component of the first harmonic of the modulation frequency ω. Fig. 2(b) shows the demodulated frequency response signal by scanning the modulation frequency ω. The value of magnetic field B_y can be extracted from the dispersive signal. From (4), one can find that the demodulated dispersive signal is equal to zero when the laser modulation frequency is locked to Larmor frequency. So the intercept of frequency axis represents the value of the magnetic field. Fig. 2(c) shows the magnetic field noise power spectral density (PSD) of the magnetometer. To measure the magnetic noise PSD, the laser modulation frequency is detuned on resonance according to the intercept of frequency axis. The demodulated signal is recorded for 14 s at a sampling rate of 1000 points/s. Then fast Fourier transform with rectangle window is performed on the data to yield the amplitude noise PSD. According to (8), the amplitude noise PSD is converted into the magnetic field noise PSD via dividing the amplitude noise spectrum by the resonant response k_0, which can be obtained from the slope of linear fit of the data near the resonance center of the dispersive signal [20]–[22]. The sensitivity averaged in 1 Hz bins is found to be 0.5 $\text{pT}/\sqrt{\text{Hz}}$ for frequencies below 50 Hz. As predicted by the theory described in Section 3, similar experimental results can be obtained when the magnetic field is along the x direction.

When the magnetic field is along the z direction, the spin orientation created by circular component of the light is also along the z axis, so the magnetic torque on the spin orientation is equal to

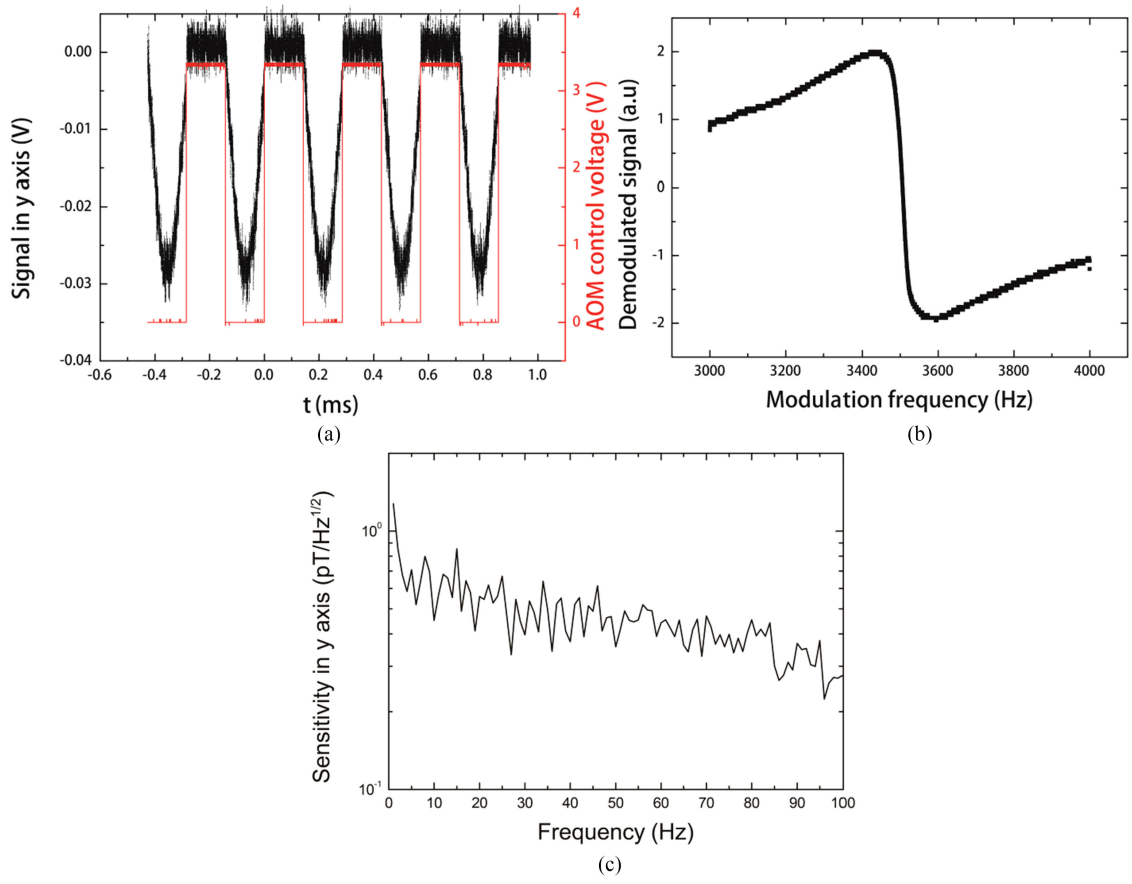

Fig. 2. (a) Time domain signal when the magnetic field is along the y direction. The red solid line represents the AOM control voltage. When the voltage lower than 2.5 V is applied to AOM, the light is switched on. The spin precession is visible during the switched-on time. (b) The frequency response signal obtained from the lock-in amplifier by scanning the modulation frequency. (c) Noise PSD of the lock-in signal converted to the units of magnetic field. The lock-in time constant and roll-off of the lock-in amplifier are set to 1 ms and 24 dB/octave , respectively. The power and ellipticity of the light are 20 μw and 22.5°, respectively. The frequency of the light is red detuned by 250 MHz from the $F = 2 \rightarrow F' = 1$ transition.

zero. The spin orientation Bell-Bloom magnetometer doesn't work. But the elliptically polarized light can also optically pump spin alignment along the y axis. When $\omega = 2\omega_L$, the spin alignment Bell-Bloom magnetic resonance occurs. In this case, the magnetometer has the typical experimental arrangements similar to magnetometer based on nonlinear magneto-optical rotation with amplitude modulated light [23]. In Fig. 3, the time domain signal, the frequency response signal and the magnetic noise PSD are shown. In the experiment, the half-wave plate is adjusted to eliminate the DC offset in the dispersive signal. Therefore, the base floor is nearly invisible in Fig. 3(b).

In this experiment, an important experimental parameter is the ellipticity ε of the elliptically polarized light. When the magnetic field is along the x or y direction, the circular component of the elliptically polarized light optically pumps the atoms while the linear component is used to measure the optical rotation. But when the magnetic field is along the z direction, only the linear component is used for both: pumping and probing. Therefore, the ellipticity of the light should be optimized for magnetometer in the three directions. Because the two cases for the magnetic field along the x and y direction are completely equivalent, we only consider the magnetic field along the y direction as an example.

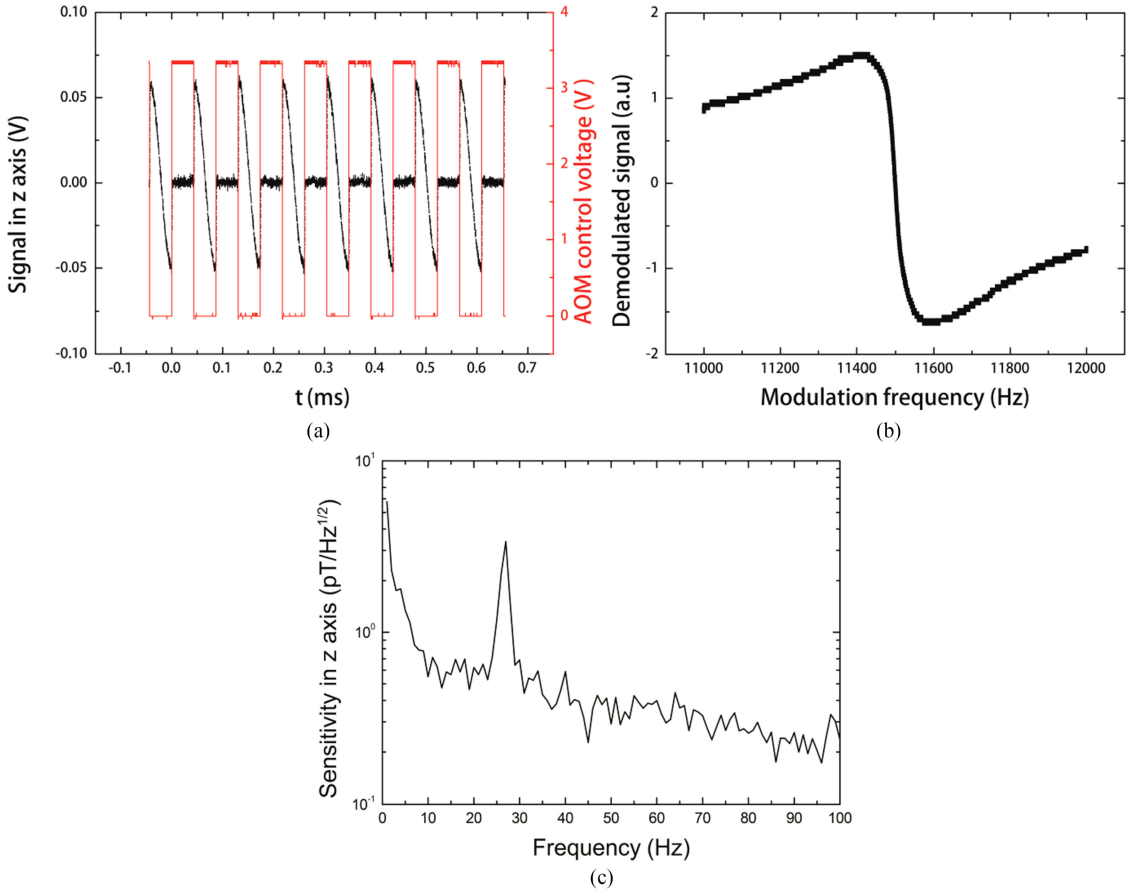

Fig. 3. (a) Time domain signal when the magnetic field is along the z direction. The red solid line represents the AOM control voltage. (b) The frequency response signal obtained from the lock-in amplifier by scanning the modulation frequency. (c) Noise PSD of the lock-in signal converted to the units of magnetic field. Except for the magnetic field direction, other experimental conditions are the same as in Fig. 2.

The dependence of magnetometer sensitivity on the ellipticity ε is measured and plotted in Fig. 4(a). It can be found that, as the ellipticity ε increases from 0° to 15°, the magnetometer sensitivity increases slowly in the z direction, whereas in the y direction the sensitivity is slightly improved. After that, there is no visible changes when ε is changed from 15° to 30°. When the ellipticity is greater than 30°, the sensitivities in both z and y directions decrease sharply. The reason of the sensitivity change in the z direction is that, when the linear component decreases gradually with the increase of the ellipticity, the sensitivity is degraded. For the sensitivity change in the y direction, according to equation (8), the sensitivity is related to the slope and noise. The slope can be expressed by the ratio of signal amplitude to the linewidth. As shown in Fig. 4(b), (c), the noise and linewidth are essentially unchanged. Therefore, the sensitivity change is determined by the amplitude. The signal amplitude has an opposite variation trend relative to the sensitivity. This change indicates there is a process of competition. As the ellipticity ε increases, higher spin polarization can be produced due to the increased circular component, which results in the larger signal amplitude. But the decreased linear component as probe beam reduces the signal amplitude. This competitive process results in the variation trend of the y direction sensitivity. The left and right signal amplitude data of Fig. 4(c) indicate linear polarization component has greater influence than circular polarization component. Fig. 4(a) shows that the sensitivities in two directions are nearly equal when the ellipticity ε varies from 15° to 30°. Therefore, in order to have the same calibration

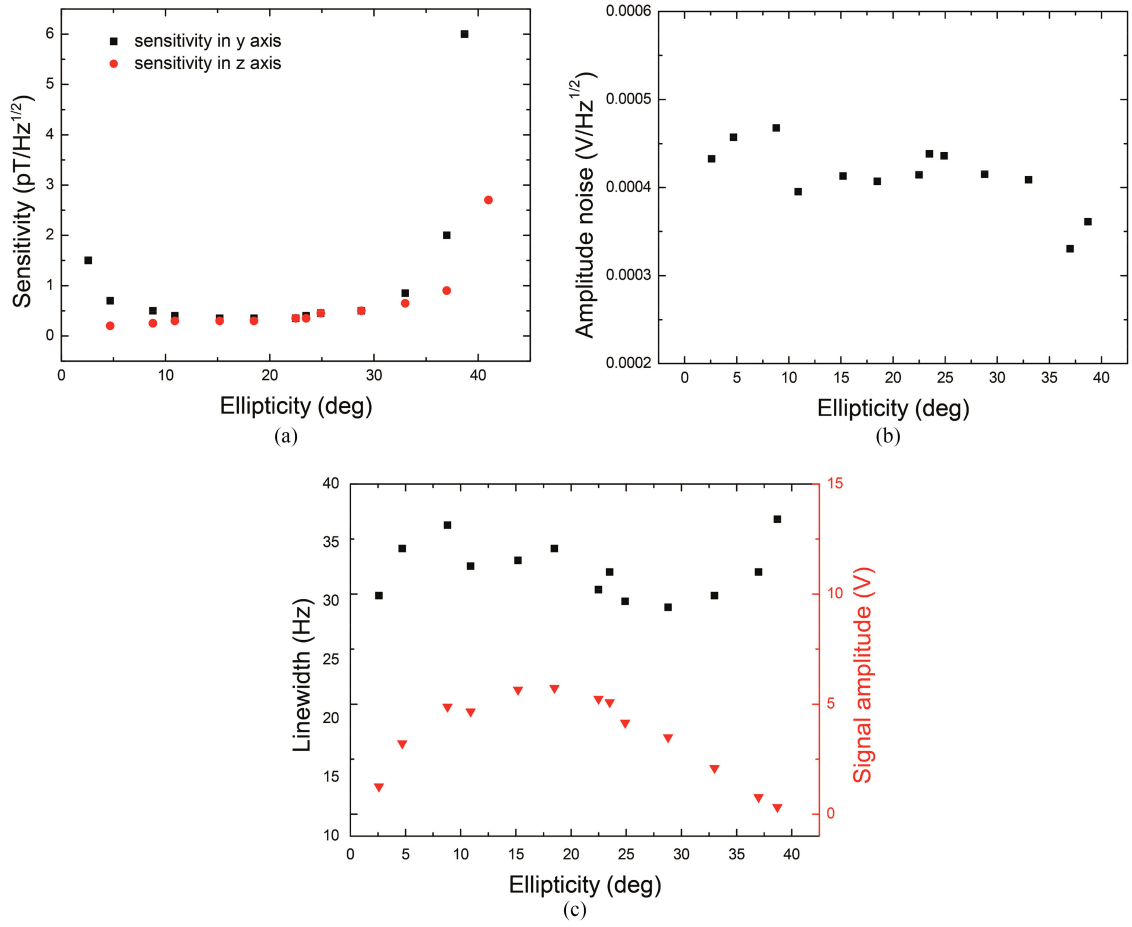

Fig. 4. (a) The magnetometer sensitivity for different ellipticity when the magnetic field is along the y direction (black square) and z direction (red circle). (b) Dependence of the amplitude noise on the ellipticity ε. (c) Dependences of the linewidth and signal amplitude on the ellipticity ε.

accuracy in the three directions, the ellipticity ε is adjusted to 22.5° for the next calibration procedure. A quantitative model may be required to explain the sensitivity change accurately, and can be a topic of future study.

We use a calibration procedure similar to the digital-locking process. First, by scanning the modulation frequency with wide span, the Larmor frequency can be located within the range of dispersive signal. Next, the modulation frequency is manually changed to set the demodulated signal equal to zero. The Larmor frequency can be found roughly. Finally, the modulation frequency is scanned with 10 Hz span and the center frequency is set to the rough Larmor frequency. The accurate Larmor frequency can be obtained from the dispersive signal with narrow span, as shown in Fig. 5(a). The beginning and end are excluded from the fitted data. Fig. 5(b) shows a typical example of calibration for B_x field coil. The curve in Fig. 5(b) shows the dependence of the magnetic field on the current in the coil, fitted linearly by the relation $B_x = c_x I_x + B_x^{res}$. The slope of the curve is the coil constant in the x axis.

There may be a phase error problem, but it just affects the residual magnetic field B_x^{res} [24]. In order to verify this point, we change the phase purposely and find that the coil constant is not affected, only the calibration curve is shifted upward by about 1 nT as shown in the inset of Fig. 5(b). The DC offset in the z direction has the same effect on the calibration of the coils, just as the phase error does. Another problem to consider is the light shift caused by the circular polarization component.

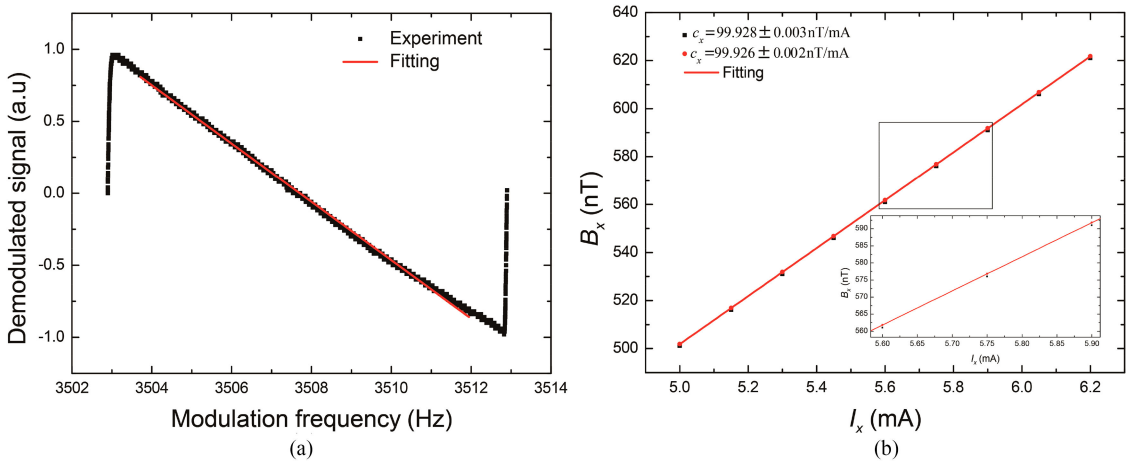

Fig. 5. (a) The frequency response signal obtained from the lock-in amplifier with 10 Hz span. (b) Dependence of the magnetic field on the applied current. The applied current is 5.0–6.2 mA at 0.15 mA intervals. The red circles represent the upward shift curve. The inset shows an enlarged view of the highlight area of the plot.

In our experiment, the power of the light is 20 μw and the frequency of the light is red detuned by 250 MHz from the $F = 2 \rightarrow F' = 1$ transition. According to the semiclassical theory of Ref. [25], [26], the magnetic field caused by the light shift is about 1nT in the z direction. In the x and y direction, the light shift is very small relative to the magnetic field along the x and y direction. Therefore, the effect can be neglected. In the z direction, the light shift adds a residual magnetic field, and hence changes the Larmor frequency. However, this effect only shifts the calibration curve by about 1 nT and does not change the slope of the calibration curve, thus will not introduce a systematic error in the coil calibration.

In the calibration procedure, measurements are repeated eight times to increase the measurement accuracy in each direction. The average of the eight calibration values yields the coil constants of $c = 99.94 \pm 0.01$ nT/mA, 99.71 ± 0.02 nT/mA, and 125.90 ± 0.08 nT/mA in the x, y and z axis, respectively. From the results, one can see that the coil constant in the z axis has a relatively large deviation. This is caused by the effect of low frequency magnetic field noise as shown in Fig. 3(c). The DC background of the z direction dispersive signal introduces more serious low frequency drift in the z direction than in the x and y directions. This leads to the inaccuracy of the magnetic field measurement. There are many reasons that cause the low frequency drift, such as the low frequency fluctuation in the applied magnetic field, the intrinsic noise in the electronics, the low frequency drift in the frequency and intensity of light [27], and so on. The low frequency drift causes the amplitude fluctuation during scanning the modulation frequency, which leads to the non-linearity in Fig. 5(a). This non-linearity affects the coil calibration accuracy. The calibration accuracy can be further improved by using different low frequency noise reduction techniques.

5. Conclusion

In this paper, we demonstrate an in situ method to calibrate a three-axis coil system using ellipticity-induced Bell-Bloom magnetometer. This method is based on simultaneously producing the spin orientation and alignment by an elliptically polarized light. The coil constants are 99.94 ± 0.01 nT/mA, 99.71 ± 0.02 nT/mA and 125.90 ± 0.08 nT/mA in the x, y and z axis, respectively. The main advantage of the method is: the coil constants in all three directions can be measured without any active adjustments. Furthermore, the method has a potential to measure the filed in all directions. It is reasonable to expect that, in the future, the method will be used to overcome the dead zone, the fundamental problem of atomic magnetometer.

References

[1] D. Budker, W. Gawlik, D. F. Kimball, S. M. Rochester, V. V. Yashchuk, and A. Weis, "Resonant nonlinear magneto-optical effects in atoms," *Rev. Mod. Phys.*, vol. 74, no. 4, pp. 1153–1201, Nov. 2002.

[2] D. Sheng, S. Li, N. Dural, and M. V. Romalis, "Subfemtotesla scalar atomic magnetometry using multipass cells," *Phys. Rev. Lett.*, vol. 110, no. 16, Apr. 2013, Art. no. 160802.

[3] Y. Ai-Lin, Y. Guo-Qing, C. Xun-Ming, X. Yun-Fei, and L. Qiang, "A laser pump-re-pump atomic magnetometer," *Chin. Phys. B*, vol. 22, no. 12, May 2013, Art. no. 120702.

[4] S.-Q. Liang, G.-Q. Yang, Y.-F. Xu, Q. Lin, Z.-H. Liu, and Z.-X. Chen, "Simultaneously improving the sensitivity and absolute accuracy of CPT magnetometer," *Opt. Exp.*, vol. 22, no. 6, pp. 6837–6843, May 2014.

[5] E. Boto *et al.*, "Moving magnetoencephalography towards real-world applications with a wearable system," *Nature*, vol. 555, no. 7698, pp. 657–661, Mar. 2018.

[6] A. P. Colombo *et al.*, "Four-channel optically pumped atomic magnetometer for magnetoencephalography," *Opt. Exp.*, vol. 24, no. 14, pp. 15403–15416, Jul. 2016.

[7] M. P. Ledbetter *et al.*, "Near-zero-field nuclear magnetic resonance," *Phys. Rev. Lett.*, vol. 107, no. 10, Sep. 2011, Art. no. 107601.

[8] M. P. Ledbetter *et al.*, "Zero-field remote detection of NMR with a microfabricated atomic magnetometer," *Proc. Nat. Acad. Sci.*, vol. 105, no. 7, pp. 2286–2290, Feb. 2008.

[9] P. W. Graham and S. Rajendran, "New observables for direct detection of axion dark matter," *Phys. Rev. D*, vol. 88, no. 3, Aug. 2013, Art. no. 035023.

[10] D. Sheng, A. Kabcenell, and M. V. Romalis, "New classes of systematic effects in gas spin comagnetometers," *Phys. Rev. Lett.*, vol. 113, no. 16, Oct. 2014, Art. no. 163002.

[11] T. W. Kornack, S. J. Smullin, S.-K. Lee, and M. V. Romalis, "A low-noise ferrite magnetic shield," *Appl. Phys. Lett.*, vol. 90, no. 22, May 2007, Art. no. 223501.

[12] G. Bison *et al.*, "A room temperature 19-channel magnetic field mapping device for cardiac signals," *Appl. Phys. Lett.*, vol. 95, no. 17, Oct. 2009, Art. no. 173701.

[13] E. Breschi, Z. Grujić, and A. Weis, "In situ calibration of magnetic field coils using free-induction decay of atomic alignment," *Appl. Phys. B*, vol. 115, no. 1, pp. 85–91, Apr. 2014.

[14] L. Chen *et al.*, "A method for calibrating coil constants by using the free induction decay of noble gases," *AIP Adv.*, vol. 7, no. 7, Jul. 2017, Art. no. 075315.

[15] S. J. Ingleby, P. F. Griffin, A. S. Arnold, M. Chouliara, and E. Riis, "High-precision control of static magnetic field magnitude, orientation, and gradient using optically pumped vapour cell magnetometry," *Rev. Sci. Instrum.*, vol. 88, no. 4, Apr. 2017, Art. no. 043109.

[16] V. Shah and M. V. Romalis, "Spin-exchange relaxation-free magnetometry using elliptically polarized light," *Phys. Rev. A*, vol. 80, no. 16, Jul. 2009, Art. no. 01341.

[17] A. Ben-Kish and M. V. Romalis, "Dead-zone-free atomic magnetometry with simultaneous excitation of orientation and alignment resonances," *Phys. Rev. Lett.*, vol. 105, no. 19, Nov. 2010, Art. no. 193601.

[18] M.-L. Wang, M.-B. Wang, G.-Y. Zhang, and K.-F. Zhao, "Study of the optimal duty cycle and pumping rate for square-wave amplitude-modulated Bell-Bloom magnetometers," *Chin. Phys. B*, vol. 25, no. 6, Apr. 2016, Art. no. 060701.

[19] D. Budker, D. F. Kimball, V. V. Yashchuk, and M. Zolotorev, "Nonlinear magneto-optical rotation with frequency-modulated light," *Phys. Rev. A*, vol. 65, no. 5, May 2002, Art. no. 055403.

[20] S. J. Smullin, I. M. Savukov, G. Vasilakis, R. K. Ghosh, and M. V. Romalis, "Low-noise high-density alkali-metal scalar magnetometer," *Phys. Rev. A*, vol. 80, no. 3, Sep. 2009, Art. no. 033420.

[21] R. Jiménez-Martínez, W. C. Griffith, S. Knappe, J. Kitching, and M. Prouty, "High-bandwidth optical magnetometer," *J. Opt. Soc. Amer. B*, vol. 29, no. 12, pp. 3398–3403, Nov. 2012.

[22] K. F. Zhao and Z. Wu, "Evanescent wave magnetometer," *Appl. Phys. Lett.*, vol. 89, no. 26, Dec. 2006, Art. no. 261113.

[23] S. Pustelny, A. Wojciechowski, M. Gring, M. Kotyrba, J. Zachorowski, and W. Gawlik, "Magnetometry based on nonlinear magneto-optical rotation with amplitude-modulated light," *J. Appl. Phys.*, vol. 103, no. 6, Mar. 2008, Art. no. 063108.

[24] A. K. Vershovskiĭ and E. B. Aleksandrov, "Phase error elimination in the M_x magnetometer and resonance line shape control in an unstable field using the technique of invariant mapping of a spin precession signal," *Opt. Spectrosc.*, vol. 100, no. 1, pp. 12–14, Jan. 2006.

[25] B. S. Mathur, H. Tang, and W. Happer, "Light shifts in the alkali atoms," *Phys. Rev.*, vol. 171, no. 1, pp. 11–19, 1968.

[26] K. F. Zhao, M. Schaden, and Z. Wu, "Method for measuring the dwell time of spin-polarized Rb atoms on coated pyrex glass surfaces using light shift," *Phys. Rev. Lett.*, vol. 103, no. 7, 2009, Art. no. 073201.

[27] I. Mateos, B. Patton, E. Zhivun, D. Budker, D. Wurm, and J. Ramos-Castro, "Noise characterization of an atomic magnetometer at sub-millihertz frequencies," *Sensors Actuators A, Phys.*, vol. 224, pp. 147–155, Apr. 2015.